International Journal of Nanomedicine

Dovepress
open access to scientific and medical research

Open Access Full Text Article

ORIGINAL RESEARCH

Doxorubicin-modified magnetic nanoparticles as a drug delivery system for magnetic resonance imaging-monitoring magnet-enhancing tumor chemotherapy

This article was published in the following Dove Press journal:
International Journal of Nanomedicine
12 May 2016
Number of times this article has been viewed

Po-Chin Liang[1,2,*]
Yung-Chu Chen[1,3,*]
Chi-Feng Chiang[1]
Lein-Ray Mo[4]
Shwu-Yuan Wei[2]
Wen-Yuan Hsieh[3]
Win-Li Lin[1,5]

[1]Institute of Biomedical Engineering, College of Medicine, College of Engineering, [2]Department of Medical Imaging, National Taiwan University Hospital, Taipei, [3]Biomedical Technology and Device Research Labs, Industrial Technology Research Institute, Hsinchu, [4]Division of Gastroenterology, Department of Internal Medicine, E-Da Hospital, Kaohsiung, [5]Institute of Biomedical Engineering and Nanomedicine, National Health Research Institutes, Miaoli, Taiwan

*These authors contributed equally in this work

Correspondence: Win-Li Lin
Institute of Biomedical Engineering, College of Medicine, College of Engineering, National Taiwan University, No 1, Section 1, Jen-Ai Road, Taipei 100, Taiwan
Tel +886 2 2312 3456 ext 81445
Fax +886 2 2394 0049
Email winli@ntu.edu.tw

Wen-Yuan Hsieh
Biomedical Technology and Device Research Labs, Industrial Technology Research Institute, No 195, Section 4, Chung Hsing Road, Chutung, Hsinchu 31040, Taiwan
Tel +886 3 591 8143
Email hsiehw@itri.org.tw

Abstract: In this study, we developed functionalized superparamagnetic iron oxide (SPIO) nanoparticles consisting of a magnetic Fe_3O_4 core and a shell of aqueous stable polyethylene glycol (PEG) conjugated with doxorubicin (Dox) (SPIO-PEG-D) for tumor magnetic resonance imaging (MRI) enhancement and chemotherapy. The size of SPIO nanoparticles was ~10 nm, which was visualized by transmission electron microscope. The hysteresis curve, generated with vibrating-sample magnetometer, showed that SPIO-PEG-D was superparamagnetic with an insignificant hysteresis. The transverse relaxivity (r_2) for SPIO-PEG-D was significantly higher than the longitudinal relaxivity (r_1) ($r_2/r_1 > 10$). The half-life of Dox in blood circulation was prolonged by conjugating Dox on the surface of SPIO with PEG to reduce its degradation. The in vitro experiment showed that SPIO-PEG-D could cause DNA crosslink more serious, resulting in a lower DNA expression and a higher cell apoptosis for HT-29 cancer cells. The Prussian blue staining study showed that the tumors treated with SPIO-PEG-D under a magnetic field had a much higher intratumoral iron density than the tumors treated with SPIO-PEG-D alone. The in vivo MRI study showed that the T_2-weighted signal enhancement was stronger for the group under a magnetic field, indicating that it had a better accumulation of SPIO-PEG-D in tumor tissues. In the anticancer efficiency study for SPIO-PEG-D, the results showed that there was a significantly smaller tumor size for the group with a magnetic field than the group without. The in vivo experiments also showed that this drug delivery system combined with a local magnetic field could reduce the side effects of cardiotoxicity and hepatotoxicity. The results showed that the developed SPIO-PEG-D nanoparticles own a great potential for MRI-monitoring magnet-enhancing tumor chemotherapy.

Keywords: superparamagnetic iron oxide, polyethylene glycol, doxorubicin, MRI monitoring, magnet enhancing, chemotherapy

Introduction

In the past, nanoparticles have been developed for their great potential application in drug delivery systems and tumor diagnosis.[1–5] The development of multifunctional nanoparticles for the delivery of both therapeutic and contrast agents to cancer tumors would be possible for tumor theranostics.[6–8] In addition, nanoparticles offer many functions, such as combining magnetic resonance imaging (MRI) contrast agent, chemotherapeutics, and active targeting, in one nanocarrier, representing a novel strategy in nanomedicine.[9–12]

Doxorubicin (Dox) is one of the most effective anticancer drugs against many types of cancer tumors. However, its clinical application is limited by its side effects

and drug resistance. Consequently, many new nanocarriers, such as polymeric nanoparticles,[13,14] are widely used to reduce the side effects of anticancer drugs and improve their half-life in blood circulation. However, these systems cannot be controlled to release drugs accurately. Therefore, it is important to combine the nanocarrier with a targeting method to reduce the side effects of the anticancer drugs on healthy organs.

Superparamagnetic iron oxide (SPIO) nanoparticles possess specific magnetic properties as being an effective contrast agent for MRI to increase the detection and characterization of tumor lesions within the body. The magnetic property of SPIO nanoparticles (SPIONs) can also be used as a magnetically guided drug delivery method for a lesion-targeting system. Magnetic nanoparticles are actively being developed based on their unique properties responsive to magnetic fields, including magnetic hyperthermia and MRI contrast agent.[15–18] Active targeting for superficial tumors can also be performed using magnetic fields.[19–22] This strategy has been tested in patients with advanced stages of cancer.[23,24] Many targeting studies[25–28] were focused on the magnetic particles as drug carriers, but the half-life of these particles is very short, restricting their use through the systemic route. Magnetic vehicles are attractive for the targeting delivery of therapeutic agents to specific locations in the body through the application of a magnetic field. The magnetic localization of therapeutic agents results in a higher concentration of the therapeutics at the target site and consequently reduces the side effects of systemic drug administration. The first clinical cancer therapy trials in humans using magnetic particles were reported and involved treatment of advanced solid liver cancer in 14 patients.[28] The results showed that the magnetic particles accumulated in the magnetic target area and were nontoxic.[28] The targeting using magnetic drug nanocarriers could provide a higher drug accumulation at tumor sites for cancer therapy with a lower therapeutic dose.[27,28]

Although SPIO is a well-known drug carrier, it has many disadvantages, such as low water solubility and a lack of targeting ability. Therefore, it is important to combine the nanocarrier with a targeting modality to reduce the side effects of chemotherapeutic agents on normal organs. The biocompatibility of polymers, such as polyethylene glycol (PEG), has been demonstrated both in vivo and in vitro, and such compounds have been applied to tissue engineering. Imparting a stealth shielding on the surface of nanoparticles can prevent opsonization by the reticuloendothelial system (RES) cells and then increase the circulation time from minutes to hours or days.[29] PEG modification has emerged as a customary method to ensure stealth shielding and to improve the circulation time of therapeutic agents or delivery devices. The hydrophilic PEG can improve the biocompatibility of the delivery system because most of the biological environment is hydrophilic, and biocompatibility appears to be correlated with the degree of hydrophilicity exhibiting on the surface.

In this study, we developed multifunctional SPIONs consisting of a magnetic Fe_3O_4 core and a shell of aqueous stable PEG conjugated with Dox (SPIO-PEG-D) for tumor MRI-monitoring chemotherapy. One of the major advantages for SPIO with PEG (SPIO-PEG) as a drug carrier is that the degradation of Dox could be effectively reduced by conjugating Dox on the surface of SPIO-PEG. The degree of freedom of Dox on SPIO-PEG was limited to prevent its molecular distortion and hence increase its half-life. In addition, SPIO-PEG-D could cause DNA crosslink more serious, resulting in a lower DNA expression and a higher cancer cell apoptosis. Finally, the accumulation of SPIO-PEG-D in cancer tumors could be enhanced by applying a magnetic field in the tumor to increase the degree of DNA crosslink and to reduce the damage of normal organs. This functionalized nanoparticle with high payload of Dox, high superparamagnetic property, and high MRI relaxivity could not only be an effective magnetic targeting carrier for anticancer drug but also be a great MRI contrast agent. Figure 1 shows how the developed functionalized, magnetic nanoparticles can achieve the objective of improving the drug transport to tumors.

Methods and materials

Materials

Dox HCl was obtained from Seedchem (Melbourne, Australia). Succinic anhydride, 4-dimethylamino-pyridine, sodium hydroxide, PEG (MW =2,000 Da), 2-(*N*-morpholino)ethanesulfonic acid hydrate (MES), thionyl chloride, triethylamine, 3-aminopropyl triethoxysilane, 1-ethyl-3-(3-(dimethylamino)-propyl)carbodiimide, and *N*-hydroxysulfosuccinimide were purchased from Sigma-Aldrich (St Louis, MO, USA) and used as received. Iron(III) chloride ($FeCl_3$) 99% pure granulated and iron(II) chloride tetrahydrate ($FeCl_2{\cdot}4H_2O$) were purchased from Merck (Whitehouse Station, NJ, USA). Oleic acid (IO), dichloromethane, isopropyl ether, and toluene were purchased from Thermo Fisher Scientific (Waltham, MA, USA).

Synthesis of HOOC-PEG-triethoxysilane (HOOC-PEG silane)

Fifty grams of PEG, 2.6 g of succinic anhydride, and 0.6 g of 4-dimethylamino-pyridine were dissolved in 150 mL of dichloromethane at 30°C and stirred for 24 hours to form

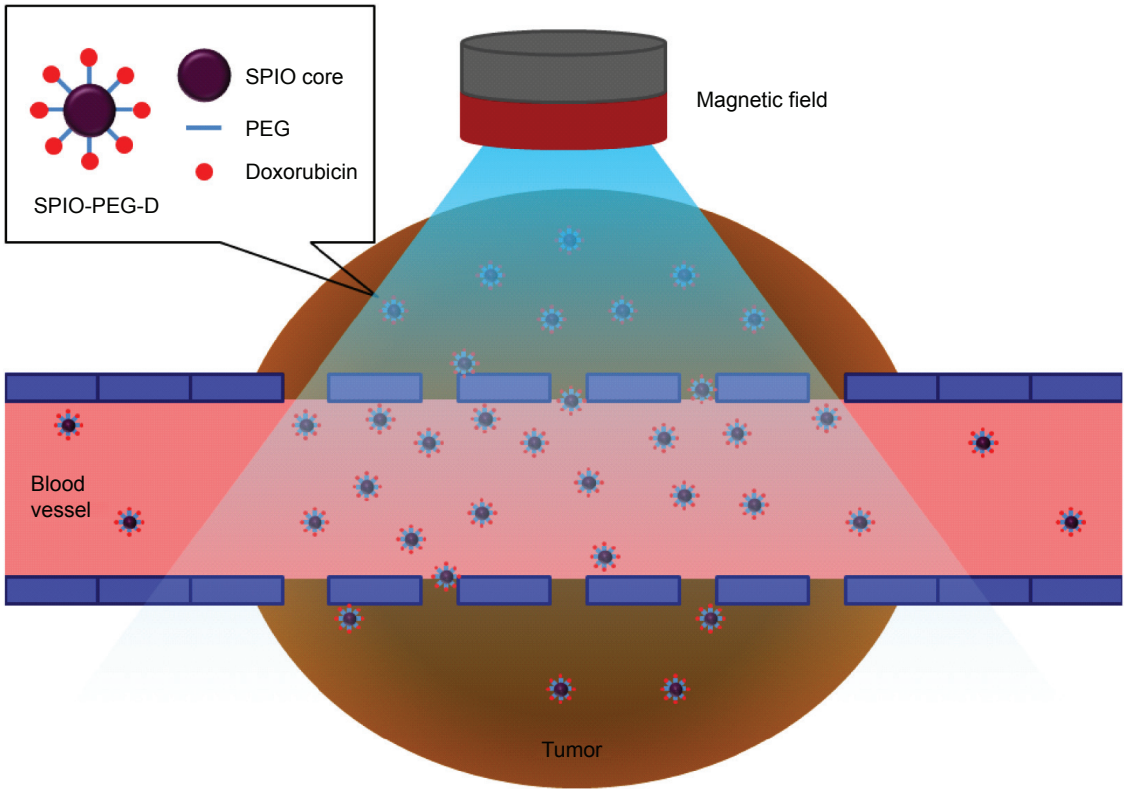

Figure 1 SPIO nanoparticles conjugated with PEG and then doxorubicin under a magnetic field during tumor treatment.
Abbreviations: SPIO, superparamagnetic iron oxide; PEG, polyethylene glycol; SPIO-PEG-D, SPIO with PEG conjugated with doxorubicin.

PEG-carboxylate. A 0.45 mL of thionyl chloride was added to the PEG-carboxylate solution at 30°C. Then, triethylamine was added to adjust the solution pH to be ~5. A total of 1.5 mL of 3-aminopropyl triethoxysilane was added to the solution mixture at 30°C, and the mixture was stirred for 10 hours. The HOOC-PEG-triethoxysilane was crystallized with isopropyl ether and dried under vacuum. The synthetic scheme of the HOOC-PEG silane is shown in Figure 2.

Synthesis of magnetite nanoparticles with IO

Ferric chloride (30 mmol) and ferrous chloride tetrahydrate (15 mmol) were dissolved in 50 mL of water. One-normal sodium hydroxide solution was added to the mixture solution until pH reached 12. Five milliliters of IO was added to the dark solution and formed a black precipitate. The precipitate was centrifuged at 6,000 rpm for 10 minutes, washed with water, and isolated as black pellet. The pellet was redispersed in water, and the pH of solution was adjusted to 4 using 6 N HCl. The resulting mixture was centrifuged at 9,000 rpm for 30 minutes to collect dark precipitate and dried under vacuum for 2 days. The dark solid was redispersed in toluene and centrifuged at 9,000 rpm for 30 minutes to collect the supernatant. The supernatant was filtered through 0.45 µm polytetrafluoroethylene filter and collected as an IO nanoparticle suspension solution.

Synthesis of SPIO-PEG

Six grams of HOOC-PEG-triethoxysilane was added to the IO nanoparticle solution and vigorously stirred for 1 day. The resultant HOOC-PEG-immobilized IO nanoparticles were extracted with 2,000 mL of water, and the aqueous layers were collected. The SPIO-PEG nanoparticles in aqueous solution were washed, purified, and concentrated with ultrafiltration. The Fe concentration of the purified SPIO-PEG solution was determined by inductively coupled plasma spectroscopy. The SPIO-PEG powder was obtained by lyophilization and was analyzed with thermogravimetric analyzer (PerkinElmer Pyris 1; PerkinElmer, Waltham, MA, USA). The thermogravimetric analyses were carried out with 5 mg of SPIO-PEG powder, and the SPIO-PEG powder was heated from 25°C to 850°C at a heating rate of 10°C/min.

Synthesis of SPIO-PEG-D

Twenty-five milligrams of 1-ethyl-3-(3-(dimethylamino)-propyl)carbodiimide and 28 mg of *N*-hydroxysulfosuccinimide were dissolved in 1.5 mL of 0.5 M MES, and then 0.2 mL of the solution was mixed with 0.2 mL of SPIO-PEG

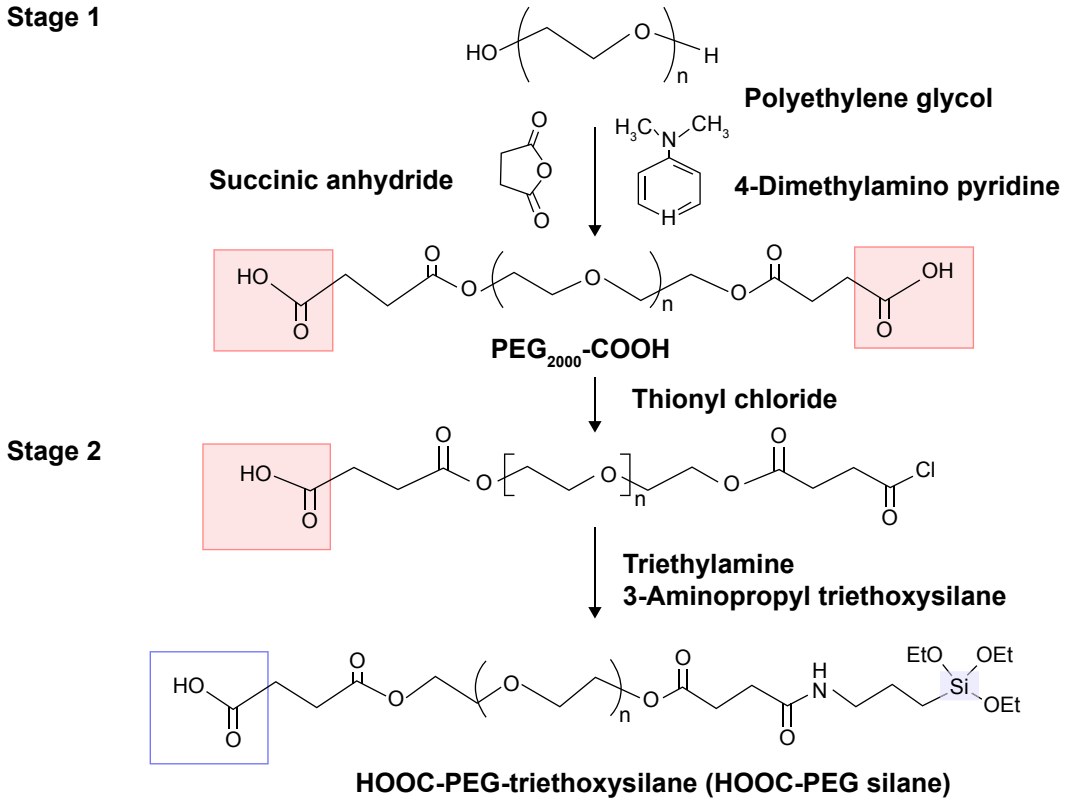

Figure 2 Synthetic route for HOOC-PEG silane.
Abbreviation: PEG, polyethylene glycol.

solution at 4°C and sonicated for 30 minutes. After that, the aqueous solution was washed with 1 mL of 0.1 M MES buffer and then resuspended in 0.3 mL of MES. The resulting mixture was mixed with 0.1 mL of Dox by vortexing for 6 hours at 4°C. The amino groups of Dox reacted with active ester and resulted in covalent conjugation of Dox on the SPIO-PEG surface. Finally, the solution was washed with water to remove unbound Dox and dispersed in 0.3 mL of water. The binding capacity of Dox was analyzed using high-performance liquid chromatography (HPLC), and the mobile phase was a 50/15/35 (v/v/v) mixture of water, acetonitrile, and methanol with a flow rate of 1.5 mL/min. The synthetic route for SPIO-PEG-D is shown in Figure 3.

Analysis of particle properties

The core particle size of SPIO-PEG and SPIO-PEG-D nanoparticles was analyzed by a transmission electron microscope (TEM) (JEM-2010HR; JEOL, Tokyo, Japan). The mean hydrodynamic diameter of SPIO-PEG and SPIO-PEG-D nanoparticles was analyzed by dynamic laser light scattering (Malvern Zetasizer 3000HSA; Malvern Instruments, Malvern, UK) at a fixed angle of 90° and a temperature of 25°C. The zeta potential of SPIO-PEG and SPIO-PEG-D nanoparticles was measured using Zetasizer Nano ZS (Malvern Instruments). The crystal lattice properties of nanoparticles were detected by X-ray powder diffraction (Siemens D5000) with the monochromatized Cu K radiation. The magnetic properties were measured with vibrating-sample magnetometer (model 7300; Lakeshore, Westerville, OH, USA). The longitudinal (r_1) and transverse relaxivities (r_2) of nanoparticles and the magnetic relaxation time (T_1, T_2) of particle solutions were measured out on a 0.47 T 20 MHz Bruker Minispec (Bruker Medical GmbH, Ettlingen, Germany). The nanoparticle were prepared by dilution to final Fe concentrations ranging from 0.1 to 0.5 mM in water. The r_1 and r_2 relaxivities were calculated from the slope of $1/T_1$ and $1/T_2$ plotted against the Fe concentration. A liquid sample of stock solution was used for the Fourier transform infrared spectroscopy analysis (TENSOR Model 27; Bruker Medical GmbH).

MRI analysis of nanoparticles in cancer cells

HT-29 human colon carcinoma cells (Bioresource Collection and Research Center, Taiwan) were grown in astrocyte medium. The human colon cancer cell HT-29 is an established cell line and contained no identity of the patient. Our study was not

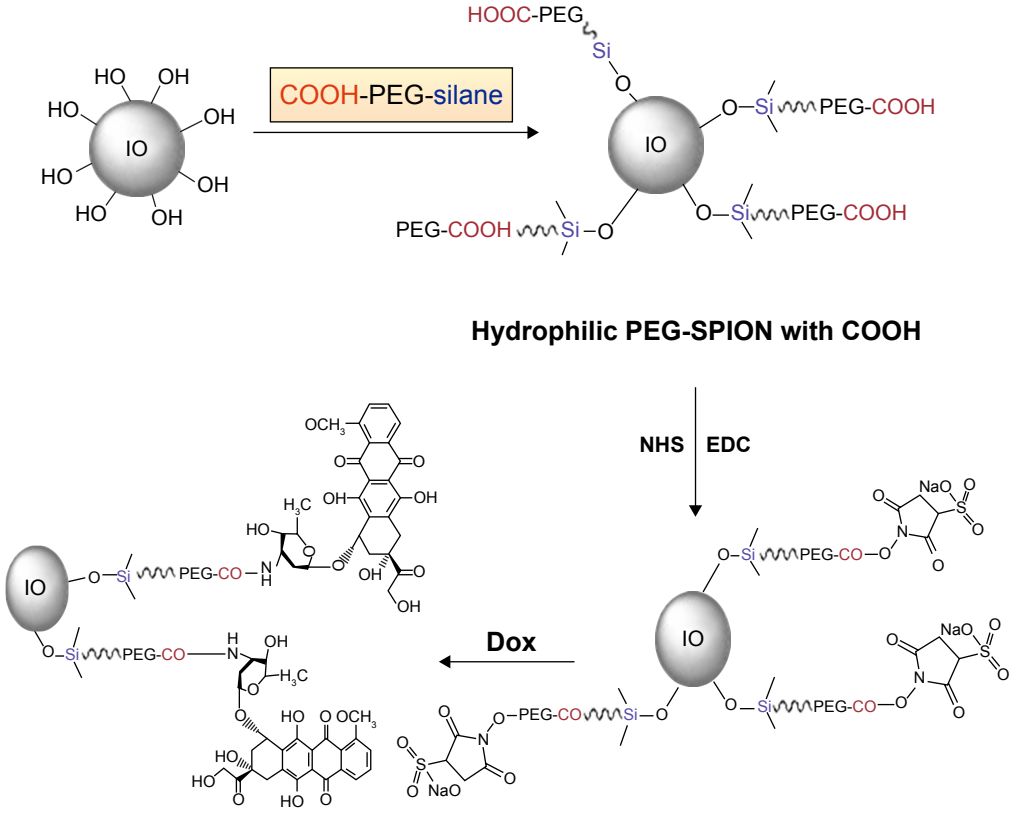

Figure 3 Synthetic route for SPIO-PEG-D.
Abbreviations: PEG, polyethylene glycol; IO, oleic acid; PEG-SPION, PEG containing superparamagnetic iron oxide nanoparticle; SPIO-PEG-D, SPIO with PEG conjugated with doxorubicin; NHS, *N*-hydroxysulfosuccinimide; EDC, 1-ethyl-3-(3-(dimethylamino)-propyl)carbodiimide; Dox, doxorubicin.

considered human subject research and did not require ethical approval from the Institutional Research Board. The cells were cultured in standard conditions (at 37°C with 5% CO_2 in a humidified incubator) and subcultured after reaching 80% confluence. HT-29 cancer cells were grown in 175 cm^2 culture flasks at a density of 1×10^5 cells per mL, and the cell internalization of nanoparticles was measured with MRI. The experiments consisted of two groups: one treated with SPIO-PEG-D alone and the other treated with SPIO-PEG-D with a 0.4 T magnet attached to the plate bottom. The SPIO-PEG-D solution was added to each well at a concentration of 50 µg Fe/mL. After incubation for 3, 6, or 24 hours, the medium was removed, and the plates were washed four times with phosphate-buffered saline (PBS) buffer and then suspended in 300 µL of 0.5% agarose gel. Finally, the samples were transferred to a 96-well plate, and MRI was performed on a 3.0 T MRI scanner (MAGNETOM Trio, A Tim System 3T; Siemens, Munich, Germany).

Qualitative and quantitative studies of cellular uptake

Prussian blue iron staining was used to visualize the cellular uptake of SPIO-PEG-D. The experiment consisted of two groups: one treated with SPIO-PEG-D alone and the other treated with SPIO-PEG-D with a 0.4 T magnet attached to the plate bottom. HT-29 cancer cells were seeded in a six-well chamber slide (1×10^5 per well) and incubated with Dulbecco's Modified Eagle's Medium and 5% fetal calf serum containing SPIO-PEG-D at a concentration of 40 µg Fe/mL for 24 hours. Then, the cells were washed with PBS buffer solution and fixed with 3% paraformaldehyde for 20 minutes. To analyze Prussian blue staining, cells were washed with PBS and incubated with 2% potassium ferrocyanide in 6% HCl. After that, the cells were washed with PBS buffer and then observed under an inverted microscope. To quantitatively determine the cellular uptake, HT-29 cancer cells were seeded in 24-well plates (1×10^5 per well) for 24 hours. The SPIO-PEG-D solution was added separately to each well at a concentration of 100 µg Fe/mL. After incubation for 0.5, 1, 3, 5, or 24 hours, the medium was removed, and the plates were washed with PBS buffer solution. Then, the cells were trypsinized and counted using a hemocytometer. The cell suspension was centrifuged at 2,000 rpm for 5 minutes to form cell pellets, and then 2 mL of hydrochloric acid was added to each pellet. After that,

the mixture solution was heated to 80°C for 5 minutes and diluted with water. Finally, all samples were analyzed using inductively coupled plasma mass spectrometer (Agilent ICP-MS 7500).

Degradation test for free Dox and SPIO-PEG-D

The mobile phase was a 50/50 (v/v) mixture of acetonitrile and mixture solution containing sodium lauryl sulfate (10 g), 80% phosphoric acid (2.5 mL), and water (1,000 mL) with a flow rate of 1.0 mL/min. The ultraviolet (UV) detection was performed at 298 nm, and the internal standard was a 50 mg/mL of papaverini hydrochloridum solution. The degradation of free Dox (FD) and SPIO-PEG-D was analyzed for a period of 114 hours at 37°C.

DNA interstrand crosslink

The ethidium bromide fluorescence assay was used to analyze the degree of DNA interstrand crosslink for HT-29 cells to assess the cytotoxic effects of Dox. The cells were exposed to 1–7 μM of FD or SPIO-PEG-D and incubated for 24 hours. Then, 1×10^5 cells were collected by centrifugation at 5,000 rpm for 10 minutes at 5°C. Forty milliliters of the cell suspension was incubated for 20 minutes at 4°C with 200 mL of lysis buffer. Then, the cell pellets were separated by centrifugation at 5,000 rpm for 10 minutes and incubated with 30 mL of heparin for 30 minutes at 37°C. After that, 1 mL of ethidium bromide solution was added in the mixture, and the mixture was heated for 10 minutes at 100°C. Finally, the mixture was cooled in an ice bath for 10 minutes, and fluorescence of all samples was measured with excitation and emission wavelengths of 525 and 580 nm, respectively.

Cell MTT cytotoxicity

MTT cytotoxicity test was used to analyze the cytotoxic effect of SPIO-PEG-D nanoparticles on cancer cells. HT-29 cells were seeded on a 96-well plate at a density of 1×10^5 cells/well in 100 μL of Dulbecco's Modified Eagle's Medium containing 5% fetal calf serum for 24 hours. The concentration range of Dox was from 1 to 10 μM. Cells incubated without any drug were used as the blank control group. The experiments consisted of three groups: FD, SPIO-PEG-D alone, and SPIO-PEG-D with a 0.4 T magnetic field. After treatment, the cells were incubated for 5 hours, and 5 mg/mL of 3-(4,5-dimethylthiazol-2-yl)-2,5-diphenyl tetrazolium bromide was added (20 μL/well) and incubated for 5 hours. The HT-29 cancer cells were then lysed with dimethylsulfoxide (100 μL) and placed in the incubator at 37°C overnight. The absorbance values of lysed cells were detected by a microplate reader (model 680; Bio-Rad Laboratories Inc., Hercules, CA, USA) at a wavelength of 490 nm.

In vivo MR image and detection of iron

Male Sprague Dawley rats (180–190 g) were obtained from the National Laboratory Animal Center (Taiwan). All experimental protocols were approved by the Institutional Animal Care and Use Committee of the College of Medicine, National Taiwan University. The rats were housed with a 12-hour light/dark cycle and allowed free access to water and standard diet. CT-26 cancer cells were transplanted subcutaneously into the right and left thigh of the rats (6×10^6 cells/0.1 mL). Sixteen tumor-bearing rats were randomly divided into two groups (12 and 24 hours) for the in vivo MR image experiment. Seven days later, sixteen rats were intravenously injected with SPIO-PEG-D nanoparticles (18 mg Fe/kg) and then with a 0.4 T magnet secured to the left thigh for 12 or 24 hours. The rats were assessed longitudinally by MR image after treatment to determine the tumor size. The MR images were acquired on a 3 T scanner (Trio with Tim; Siemens) and quantified using T_2-weighted images with the following parameters: repetition time =4,230 ms, echo time =96 ms, slice thickness =1 mm, field of view 48×75 mm, bandwidth 260 Hz/px, resolution =164×256, averages =2, and total scan time =1 minute 37 seconds. After that, male rats bearing tumor were treated with SPIO-PEG-D or SPIO-PEG-D under a 0.4 T magnetic field (SPIO-PEG-D/MF) at a dose of 18 mg/kg Dox. The animals were perfused with saline and 4% paraformaldehyde at 24 hours after the SPIO-PEG-D administration. Tumors were extracted and immersed in the same fixative solution for 4 hours. Before analysis, the tumor tissue was embedded in Tissue-Tek optimum cutting temperature compound (Thermo Fischer Scientific, Waltham, MA, USA) on a specimen disk and cryo-frozen immediately in liquid nitrogen. Subsequently, the tumor tissue was sectioned into 20 μm thick slices with microtome (Cryostat, Leica CM3050s; Leica Biosystems, Wetzlar, Germany). The tumor tissue slices were dried on the gelatin-coated microscopic slides. The slides were rinsed three times and mounted using the Dako Fluorescence Mounting Medium (Dako, Glostrup, Denmark). The tumor tissue sections were imaged under Olympus FV1000 confocal microscope (Olympus, Tokyo, Japan). After that, the tumor tissues were fixed in 10% neutral buffered formalin, processed, and embedded with paraffin for detection of iron expression by Prussian blue staining. The tumor tissues were fixed in phosphate buffer containing 25 mg/mL glutaraldehyde, postfixed in 10 mg/mL osmium tetroxide,

dehydrated in alcohol, and embedded for cellular uptake analysis. Finally, the sections were stained with uranyl acetate and lead citrate and then examined using a TEM.

In vivo antitumor activity

Female BALB/c nude mice (30±2 g) were obtained from the National Laboratory Animal Center (Taiwan). HT-29 cancer cells were transplanted subcutaneously into the abdomen of mice (1×10^5 cells/0.1 mL). Seven days later (size of tumor: ~60 mm^3), the experiments were executed for three groups (n=4 for each group): one group intravenously injected with FD (2.5 mg Dox/kg), another group injected with SPIO-PEG-D nanoparticles (2.5 mg Dox/kg) alone, and the other group injected at the same dose of SPIO-PEG-D and a 0.4 T magnet secured to the hypodermic tumor for 24 hours. The administration was carried out seven times with a 3-day interval for each mouse. The tumor size was calculated by the formula $a\times b^2/2$, with a and b being the longest and shortest diameter, respectively.

Apoptosis detection for tumor cells

The treated mice were sacrificed for apoptosis detection on day 40 after tumor implantation. After sacrifice, the mice were perfused using transcardiac method with 10% neutral buffered formalin. Tumor, heart, kidney, and liver tissues were collected and fixed with 10% neutral buffered formalin for at least 48 hours. The apoptotic cells in tissues were detected with terminal deoxynucleotidyl transferase dUTP nick-end labeling (TUNEL) assays using an in situ cell death detection kit and observed using Olympus FV1000 confocal microscope (Olympus).

Results and discussion

Synthesis of HOOC-PEG-triethoxysilane (HOOC-PEG silane) and thermal properties of nanoparticles

HOOC-PEG silane was analyzed by ^{1}H NMR spectroscopy using a 400 MHz Bruker spectrometer (AVANCE model; Bruker) at 25°C, and the result is shown in Figure 4A. ^{1}H NMR ($CDCl_3$, δ in ppm): 4.05 (brm, CH_2CH_2OCO–), 3.77 (quart, –$SiOCH_2CH_3$–), 3.46 (brm, –CH_2CH_2O–), 3.24 (brm, –$NHCH_2CH_2CH_2Si$–), 1.80 (brm, –$NHCH_2CH_2CH_2Si$–), 1.15 (trip, –$SiOCH_2CH_3$–), 0.55 (brm, –$NHCH_2CH_2CH_2Si$–). Figure 4B shows the dynamic thermogravimetric curves of SPIO-PEG nanoparticles. The initial 5% of total weight loss was due to the residual water. The 75% of total weight loss between 250°C and 450°C was attributed to the thermal degradation of PEG coated on the SPIO surface. The 20% of residual weight after 750°C was counted as the iron oxide.

Characterization of nanoparticles

Figure 5 shows the particle size of SPIO-PEG and SPIO-PEG-D nanoparticles. The TEM images displayed the core particle size and morphology for both SPIO-PEG and SPIO-PEG-D nanoparticles. The size of core particles is ~6–10 nm on average for both SPIO-PEG and SPIO-PEG-D nanoparticles, and the high-resolution TEM micrograph showed that the core particles of both SPIO-PEG and SPIO-PEG-D were spherical in shape. The hydrodynamic diameter indicated that the average particle size was ~70 and 85 nm for SPIO-PEG and SPIO-PEG-D, respectively. The discrepancy of the measured particle sizes between dynamic laser light scattering and TEM is a hydrophilic PEG layer conjugated on the surface of nanoparticles. The PEG layer increases the hydrodynamic diameter due to the flexibility of the PEG backbone.[30–32] Table 1 shows the characterization of SPIO-PEG and SPIO-PEG-D. The hydrodynamic diameter was 70±2.3 and 85±3.1 nm, and polydispersity index was 0.213±0.03 and 0.242±0.05 for SPIO-PEG and SPIO-PEG-D, respectively. The zeta potential of SPIO-PEG in water was −14.2±0.4 mV, and it increased to −1.8±0.21 mV when Dox was conjugated with SPIO-PEG. SPIO-PEG-D is stable in water for a period of 12 months (Figure 5E), and the SPIO-PEG-D particles did not aggregate and change the particle size, and such stability is desirable for use in biological applications.

Qualification and quantification of SPIO-PEG-D

The characteristic absorption peaks of SPIO-PEG, Dox, and SPIO-PEG-D were confirmed by Fourier transform infrared spectroscopy analysis (Figure 6A). The O–H (3,405 cm^{-1}) and C=O (1,652 cm^{-1}) peaks are from COOH of SPIO-PEG. The N–H bond and C–O bond from Dox appear at 1,553 and 1,645 cm^{-1}, respectively. The bands at 3,427 and 3,251 cm^{-1} are attributed to NH_2 stretching band on Dox. The characteristic absorption peaks of SPIO-PEG-D showed C=O bonds at 1,692 cm^{-1}, and C–N stretching band from amide bond appears at 1,403 cm^{-1}. The peak at 3,430 cm^{-1} is attributed to N–H stretching band from amide bond. This result indicated the amide bond formation between the carboxyl groups of SPIO-PEG and the amino groups of Dox. The HPLC measurement showed that the amount of Dox conjugated with SPIO-PEG-D increased as the amount of Dox added increased and reached a saturating concentration of 520 μg Dox/mg SPIO-PEG-D (Figure 6B).

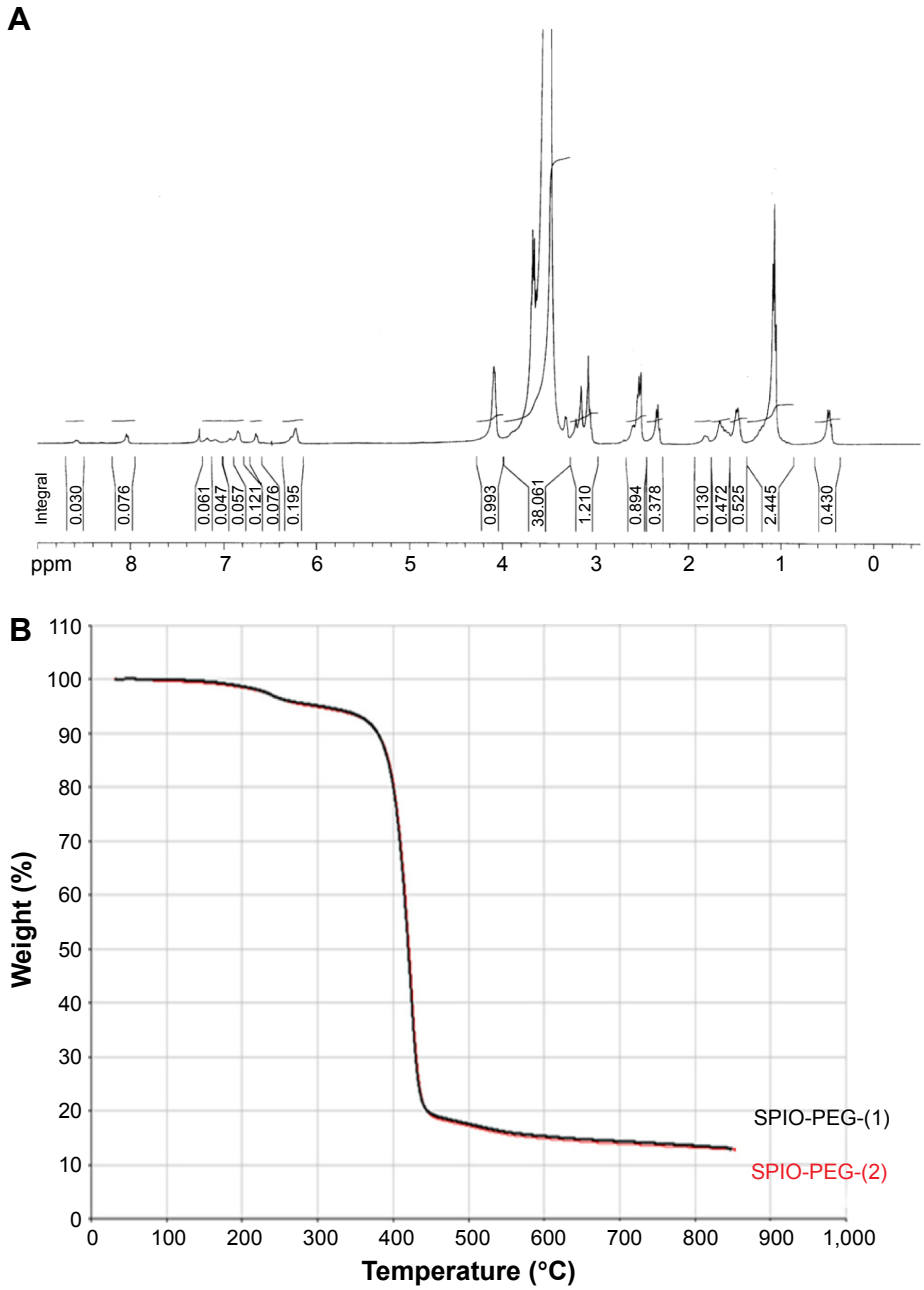

Figure 4 (**A**) ^{1}H NMR spectra for HOOC-PEG silane. (**B**) TGA curves of the SPIO-PEG were tested twice.
Abbreviations: PEG, polyethylene glycol; TGA, thermogravimetric analysis; SPIO-PEG, superparamagnetic iron oxide with PEG.

Structural analysis and magnetic properties of SPIO-PEG and SPIO-PEG-D

In Figure 7A, the X-ray diffraction of SPIO-PEG-D nanoparticles shows detectable peaks at 30.2°, 35.7°, 43.7°, 54.8°, 57.5°, and 63.1°. These peaks are similar to the characteristics of Fe_3O_4 nanoparticles.[33] The magnetic properties of SPIO-PEG and SPIO-PEG-D were evaluated by vibrating sample magnetometer and are shown in Figure 7B and C. The saturation magnetization value for SPIO-PEG and SPIO-PEG-D was 75 and 63 emu/g, respectively. The decrease of magnetization value for SPIO-PEG-D, as compared to SPIO-PEG, occurred due to the proportional decrease of Fe_3O_4 in the same mass of SPIO-PEG-D. The shape of the hysteresis curves for SPIO-PEG and SPIO-PEG-D was tight together with no significant hysteresis loss, which is expected as the behavior of superparamagnetism.[34]

Relaxivity

The longitudinal and transverse relaxation times (T_1, T_2) for SPIO-PEG and SPIO-PEG-D solutions were detected with

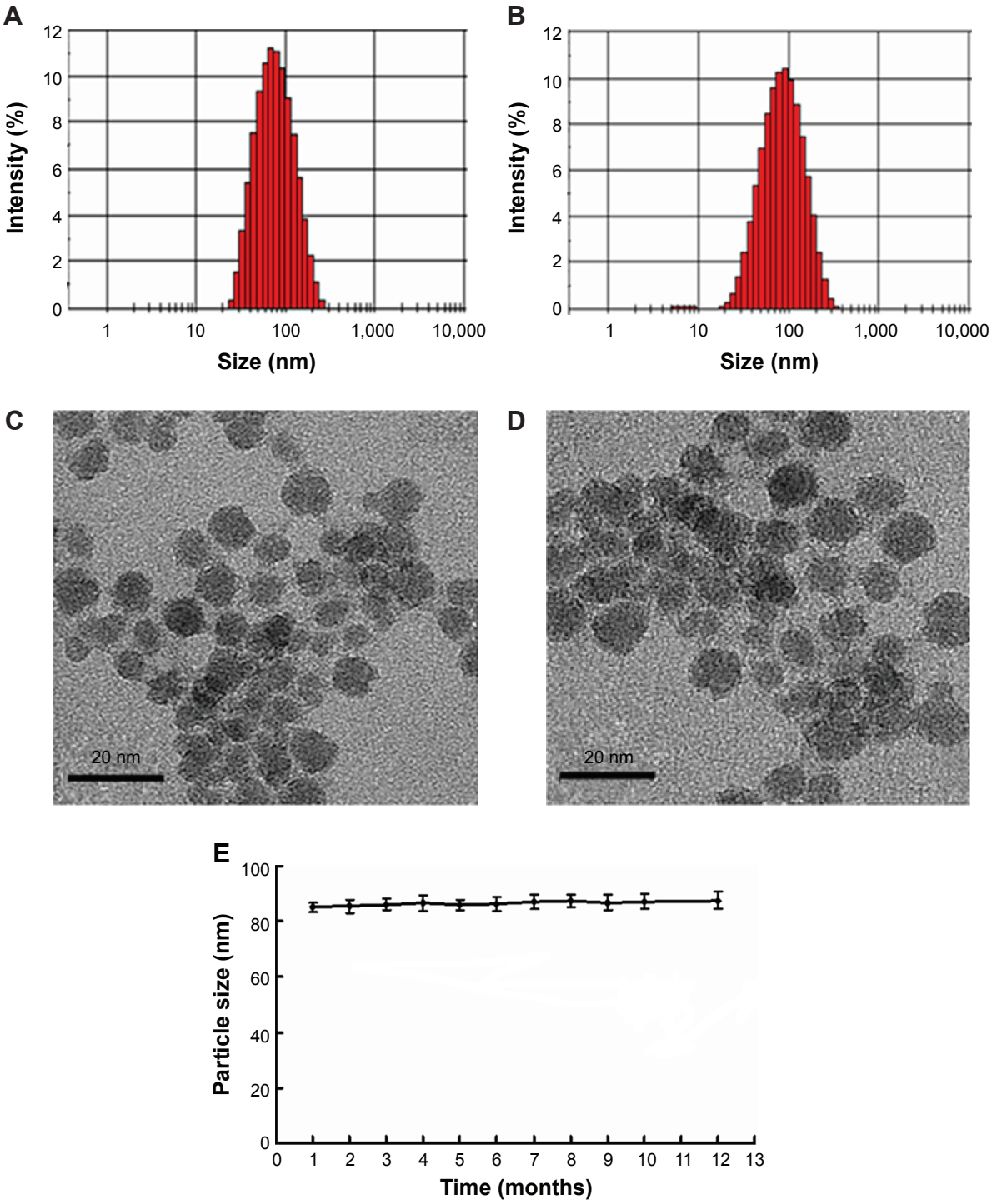

Figure 5 Particle size distribution and TEM images for (**A** and **C**) SPIO-PEG and (**B** and **D**) SPIO-PEG-D. (**E**) Stability curves of SPIO-PEG-D over 12 months (mean ± SD) (n=3).

Abbreviations: TEM, transmission electron microscope; SPIO-PEG, superparamagnetic iron oxide with polyethylene glycol; SPIO-PEG-D, SPIO with PEG conjugated with doxorubicin; SD, standard deviation.

Table 1 Characterization of SPIO-PEG and SPIO-PEG-D (n=3)

Formulation	Hydrodynamic diameter (nm)	Polydispersity index	Zeta potential value (mV)
SPIO-PEG	70±2.3	0.213±0.03	−14.2±0.4
SPIO-PEG-D	85±3.1	0.242±0.05	−1.8±0.2

Abbreviations: SPIO-PEG, superparamagnetic iron oxide with polyethylene glycol; SPIO-PEG-D, SPIO with PEG conjugated with doxorubicin.

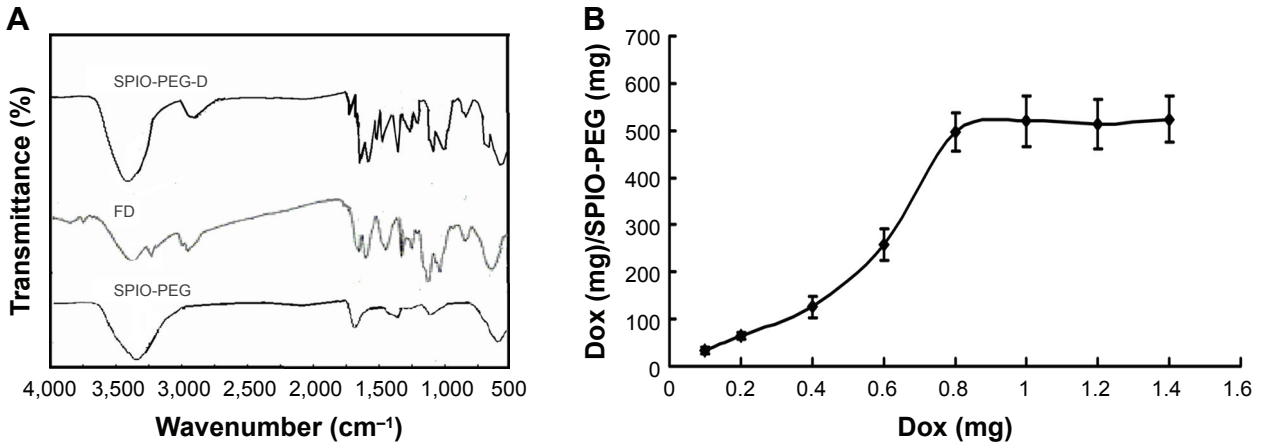

Figure 6 (**A**) FT-IR spectra for SPIO-PEG-D, Dox, and SPIO-PEG. (**B**) Quantity of Dox conjugate with SPIO-PEG.
Abbreviations: FT-IR, Fourier transform infrared; SPIO-PEG-D, superparamagnetic iron oxide with polyethylene glycol conjugated with doxorubicin; Dox, doxorubicin; SPIO-PEG, SPIO with PEG; FD, free doxorubicin.

a 0.47 T, 20 MHz magnetic relaxometer. The magnetic relaxivities (r_1, r_2) were calculated as the slope of $1/T_1$ and $1/T_2$ versus five different iron concentrations, respectively, as shown in Figure 8. There is no significant difference in r_1 between these two nanoparticles. The r_2 value of SPIO-PEG-D nanoparticles was smaller than that of SPIO-PEG, as a result of the conjugation of Dox that covers the SPIO surface and then reduces the paramagnetic effect. The result was shown in the r_2 and r_1 measurements; the r_2/r_1 ratio is 9 and 12 for SPIO-PEG-D and SPIO-PEG,

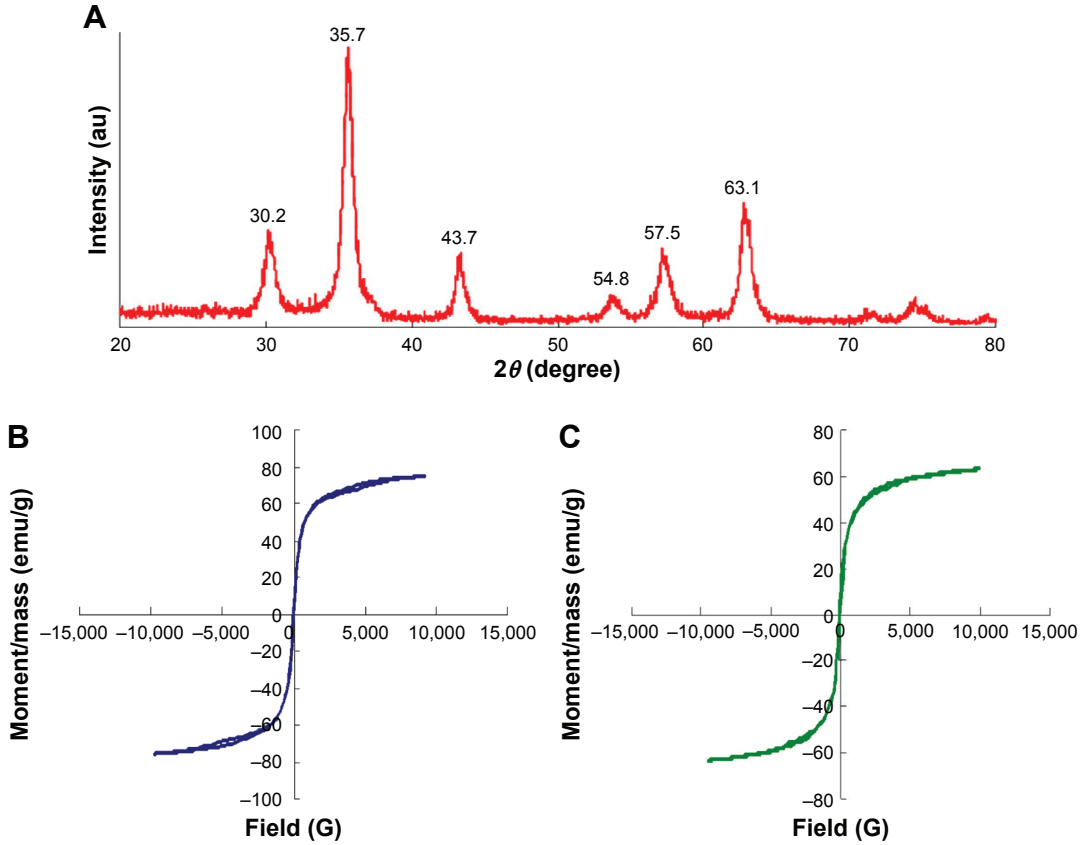

Figure 7 (**A**) X-ray powder diffraction pattern for SPIO-PEG-D, (**B**) variation of magnetization for SPIO-PEG, and (**C**) for SPIO-PEG-D as a function of applied magnetic field.
Abbreviations: SPIO-PEG-D, superparamagnetic iron oxide with polyethylene glycol conjugated with doxorubicin; SPIO-PEG, SPIO with PEG.

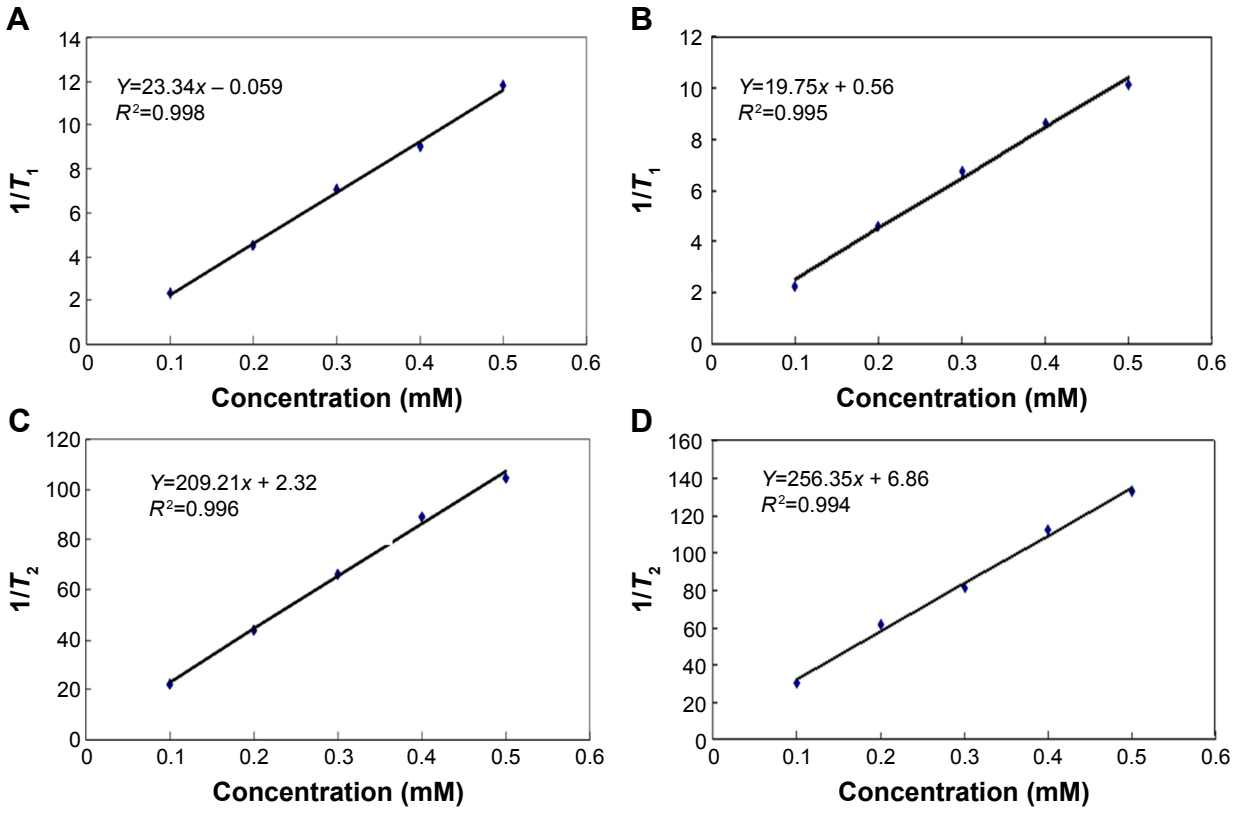

Figure 8 Relaxation response for (**A** and **B**) SPIO-PEG-D and (**C** and **D**) SPIO-PEG.
Abbreviations: SPIO-PEG-D, superparamagnetic iron oxide with polyethylene glycol conjugated with doxorubicin; SPIO-PEG, SPIO with PEG.

respectively. The r_2/r_1 ratios for both SPIO-PEG-D and SPIO-PEG were higher than Resovist® (a commercial iron oxide nanoparticle with an r_2/r_1 ratio ~7), indicating that both SPIO-PEG-D and SPIO-PEG are more effective than Resovist® as a T_2 contrast agent.

In vitro qualitative and quantitative studies of cellular uptake

MRI and cell viability were used to evaluate the potential of SPIO-PEG-D as an MR contrast agent and as an agent for magnetic-targeting chemotherapy. HT-26 cells were first incubated with SPIO-PEG-D or SPIO-PEG-D/MF for 3, 6, and 24 hours. Figure 9A shows the T_2-weighted MR images of HT-29 cells after incubation. The rapid and effective magnetic targeting leads to distinguishably darkened MR images for the SPIO-PEG-D/MF group, as compared to the SPIO-PEG-D group, at a concentration of 50 μg Fe/mL. The result also indicated that there was a significantly higher cellular uptake for the SPIO-PEG-D/MF group than the SPIO-PEG-D group, and this multifunctional drug carrier could enhance the MR sensitivity to produce a better monitoring and chemotherapy with an application of magnetic field.

Prussian blue staining studies were performed to evaluate the uptake of SPIO-PEG-D by HT-29 cancer cells, and the results are shown in Figure 9B. The figure indicates that the SPIO-PEG-D/MF group had an enhanced cellular uptake of nanoparticles, shown as a higher Fe concentration, than the SPIO-PEG-D group. The results of iron concentration inside the cancer cells are shown in Figure 9C. The SPIO-PEG-D/MF group displayed a significantly higher cellular uptake of nanoparticles by HT-29 cells than the SPIO-PEG-D group. This is because a higher accumulation of SPIO-PEG-D in the region of HT-29 cells increases the cellular internalization when the system is exposed to a magnetic field. This result demonstrated that the application of a magnetic field can positively affect the efficiency of cellular uptake for SPIO-PEG-D nanoparticles.

In vitro degradation and anticancer cell efficiency test

To determine the thermal stability of Dox conjugated to SPIO-PEG, we performed degradation analysis using HPLC. The time required for the drug degradation to be 50% of its original activity was ~68 and 96 hours for FD and SPIO-PEG-D, respectively, as shown in Figure 10A. The degree

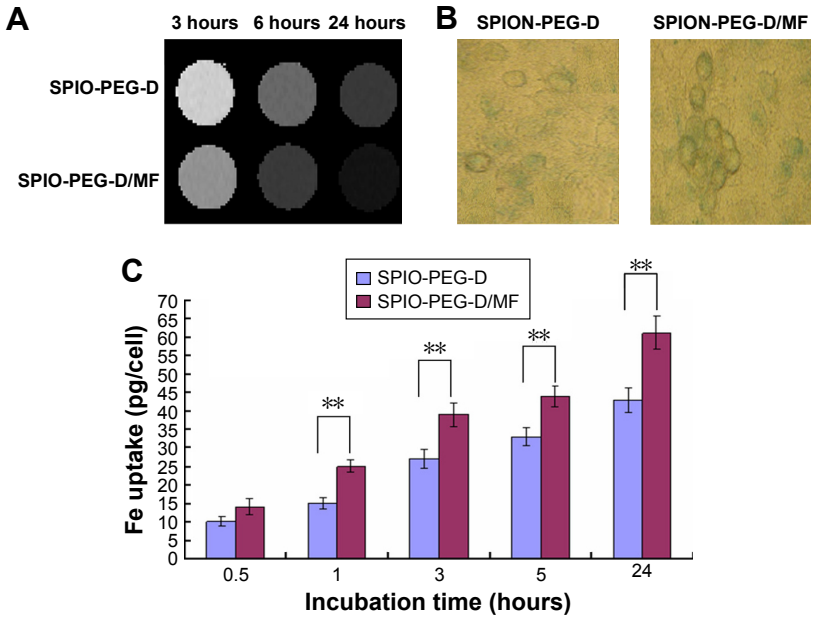

Figure 9 Cellular uptake of SPIO-PEG-D with or without magnetic field.

Notes: (**A**) T_2-weighted MR phantom images of HT-29 cells after incubation with SPIO-PEG-D or SPIO-PEG-D/MF for 3, 6, or 24 hours and (**B**) Prussian blue staining images of HT-29 cells after 24-hour treatment with SPIO-PEG-D and SPIO-PEG/MF. (**C**) The iron uptake in HT-29 cells treated with 100 μg Fe/mL of SPION-PEG-D after treatment with SPIO-PEG-D and SPIO-PEG/MF at different incubation time (mean ± SD) (n=5). $^{**}P<0.01$.

Abbreviations: MR, magnetic resonance; SPIO-PEG-D, superparamagnetic iron oxide with polyethylene glycol conjugated with doxorubicin; SPIO-PEG-D/MF, SPIO-PEG-D under magnetic field; SPIO-PEG/MF, SPIO-PEG under magnetic field; SPION-PEG-D, SPIO nanoparticle with PEG conjugated with doxorubicin; SD, standard deviation; SPION-PEG-D/MF, SPION-PEG-D under magnetic field.

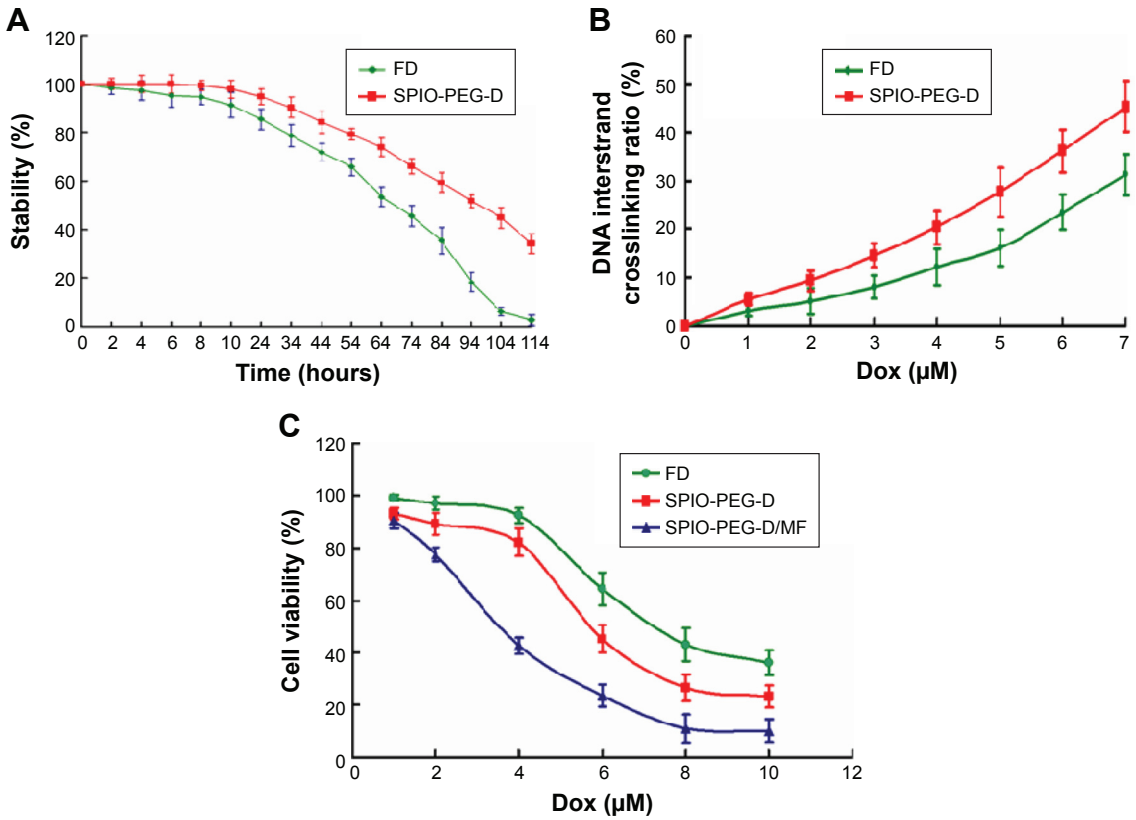

Figure 10 (**A**) Degradation curves of FD and SPIO-PEG-D over 114 hours. (**B**) DNA interstrand crosslinking in HT-29 cells after treatment with FD or SPIO-PEG-D for 24 hours. (**C**) Viability of HT-29 cells after incubation with FD, SPIO-PEG-D, or SPIO-PEG-D/MF (mean ± SD) (n=5).

Abbreviations: FD, free doxorubicin; SPIO-PEG-D, superparamagnetic iron oxide with polyethylene glycol conjugated with doxorubicin; SPIO-PEG-D/MF, SPIO-PEG-D under magnetic field; SD, standard deviation.

of Dox degradation increased for a longer incubation time at 37°C, resulting in a lower ability of crosslinking DNA. Degradation could be reduced when Dox was conjugated on the SPIO-PEG surface. The degree of freedom for Dox on SPIO-PEG was limited to significantly prevent it from molecular degradation, and therefore, its half-life of drug degradation was prolonged ~28 hours.

DNA expression and cytotoxicity effect are related to the degree of DNA interstrand crosslink. The occurrence of interstrand crosslink was 31.3% after the treatment of FD with 7 μM for 24 hours, while it increased to 45.2% (1.4-fold) for SPIO-PEG-D with the same conditions (Figure 10B). The higher degree of interstrand crosslink was correlated to an increased cytotoxicity reducing DNA expression.

The cytotoxicity of FD, SPIO-PEG-D, and SPIO-PEG-D/MF to HT-29 cells was determined using the MTT assay. Figure 10C shows that both SPIO-PEG-D and SPIO-PEG-D/MF were toxic to HT-29 cells in a dose-dependent manner. The IC50 was 5.7 and 3.6 μM for SPIO-PEG-D and SPIO-PEG-D/MF, respectively. The IC50 value was significantly reduced to 3.6 μM for the SPIO-PEG-D/MF group, presumably because more SPIO-PEG-D were driven to the cells when a 0.4 T magnetic field was applied to enhance the local drug concentration. The IC50 of FD was 6.5 μM, higher than that of SPIO-PEG-D (5.7 μM), probably because SPIO-PEG-D could cause a more serious DNA crosslink than FD, resulting in a lower DNA expression and promoting apoptosis.[35]

In vivo MR imaging and detection of iron

The short-term distribution of SPIO-PEG-D in mouse tumor tissues was assessed by T_2-weighted MR image before and after an injection of 18 mg Fe/kg, as shown in Figure 11A and B. Signal intensity in tumor decreased significantly after the injection of SPIO-PEG-D, indicating that the iron deposition in the tumor was locally increased. The in vivo MR image study also showed that the T_2-weighted signal of the SPIO-PEG-D/MF group was stronger than the SPIO-PEG-D group, indicating a better SPIO-PEG-D deposition in the tumor when a magnet was applied. The result demonstrated that a local magnetic field could help SPIO-PEG-D target the tumor and have a better retention over time. To validate the existence of SPIO-PEG-D in tumor tissues, microscopic images of Prussian blue-stained tissue slices were acquired, and the images revealed the presence of iron as shown in Figure 11C. The Prussian blue staining displayed that the SPIO-PEG-D/MF group had a much higher iron density in tumor tissues than the SPIO-PEG-D group. Figure 11C also shows confocal laser scanning microscopic images of Dox in

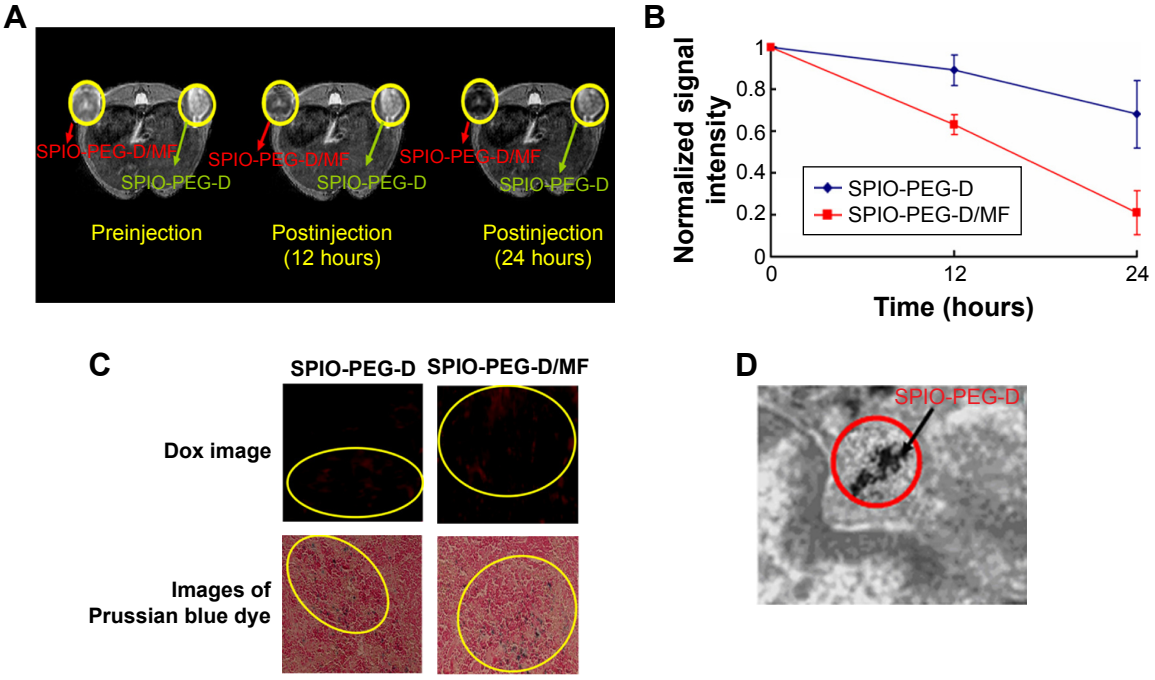

Figure 11 In vivo MR imaging and detection of SPIO-PEG-D.

Notes: (**A**) T_2-weighted MR images before and after treatment with SPIO-PEG-D (green arrows) or SPIO-PEG-D/MF (red arrows) and (**B**) MR signal intensity in mouse tumors (mean ± SD) (n=8). (**C**) Confocal laser scanning microscopic images of Dox in tumor tissues and microscope images of Prussian blue dye-stained tumor tissues after treatment with SPIO-PEG-D and SPIO-PEG-D/MF at 24 hours. Circled regions show the deposition of SPIO-PEG-D. (**D**) TEM image of tumor tissues after treatment with SPIO-PEG-D/MF. Black arrow indicates SPIO-PEG-D deposition.

Abbreviations: MR, magnetic resonance; SPIO-PEG-D, superparamagnetic iron oxide with polyethylene glycol conjugated with doxorubicin; SPIO-PEG-D/MF, SPIO-PEG-D under magnetic field; SD, standard deviation; Dox, doxorubicin; TEM, transmission electron microscope.

tumor tissues after treatment with SPIO-PEG-D at 24 hours. In Figure 11C, the signals of red fluorescence present in the coronal plane of tumor tissue sections correspond to Dox. The confocal images showed that the SPIO-PEG-D/MF group had a much higher Dox accumulation in tumor tissues than the SPIO-PEG-D group. The spatial distributions of Dox and iron oxide nanoparticles in tumors may be able to provide the information of the dissociation of Dox from SPIO-PEG-D in tumor tissues. The results show that there is a mismatch distribution for Dox and iron depositions in tumor sections. This mismatch is probably able to indicate the dissociation of Dox from SPIO-PEG-D in tumor tissues. The TEM image of selected areas showed the internalized SPIO-PEG-D in tumor cells by endocytosis, as shown in Figure 11D. Prussian blue staining and TEM images of tumor slices demonstrated that SPIO-PEG-D was guided to and retained in the tumor by applying a magnetic field.

In vivo antitumor study

Figure 12A shows the in vivo antitumor efficiency of FD, SPIO-PEG-D, and SPIO-PEG-D/MF for the tumor-bearing mice. From day 7 after tumors were implanted, FD or SPIO-PEG-D solution was administered at a dose of 2.5 mg Dox/kg, eight times with a 3-day interval. The experimental results displayed that there were 992% and 455% of tumor volume change on day 52 for the SPIO-PEG-D and SPIO-PEG-D/MF groups, respectively. The significantly better inhibition of tumor growth for SPIO-PEG-D/MF can be attributed to the application of a magnetic field in the peritumoral region, enhancing the local concentration of SPIO-PEG-D.[35] The tumor volume change for the FD group on day 40 was larger than the SPIO-PEG-D group, probably due to the Dox stability on SPIO-PEG. The increased stability could maintain activity of Dox to have interaction with topoisomerase II to form DNA-cleavable complexes and produce cytocidal activity, and this prolonged stability could be crucial to extending the therapeutic effect in vivo.[36] Notably, the body weight of mice decreased significantly during the treatment period for the SPIO-PEG-D group as shown in Figure 12B, while there was no significant change for the SPIO-PEG-D/MF group. The results demonstrated that SPIO-PEG-D/MF can enhance the tumor treatment and reduce the drug toxicity to provide a safer nanodrug delivery.

Figure 12C shows the cell apoptosis of tumor, heart, and liver tissues on day 40 after HT-29 tumor implantation, obtained from the TUNEL analysis of tissue sections from the tumor-bearing mice treated with different therapeutics. There was a significantly greater amount of apoptotic cancer cells observed in the SPIO-PEG-D/MF group than in the SPIO-PEG-D group. This is because a higher deposition of SPIO-PEG-D in the tumor region can increase the cell-killing efficacy of Dox when the tumor is exposed to a magnetic field. Figure 12A and C confirms that the magnetization of SPIO-PEG-D was an important factor for the enhancement of chemotherapy under the application of a magnet. The images of apoptotic tissues showed that the highest amount of apoptosis in heart was for the FD group and the highest amount of apoptosis in liver was for the SPIO-PEG-D group, while the TUNEL images of tissues showed that the lowest amount of apoptosis in heart and liver tissues was for the SPIO-PEG-D/MF group, suggesting that this combined system could reduce both cardiotoxicity and hepatotoxicity. SPIONs have been used as a liver-specific MRI contrast agent for detecting hepatocellular carcinoma.[37,38] This technique relies on the ability of kupffer cells to uptake SPIONs. These particles (30–200 nm) were phagocytized by macrophages of the RES, accumulating in normal liver, spleen, and lymph nodes.[39] In the liver, these particles are sequestered by phagocytic Kupffer cells in normal RES.[39] In our studies, because the particle size of SPIO-PEG-D is ~85 nm, SPIO-PEG-D was easily phagocytized by macrophages of the RES and accumulated in normal liver and spleen. The highest accumulation of SPIO-PEG-D caused the highest amount of apoptosis in liver, and the lowest accumulation of SPIO-PEG-D/MF in liver tissues could cause the lowest amount of apoptosis. Therefore, a constant strength of magnetic field could be used to guide a significant quantity of SPIO-PEG-D to tumor region to increase the local drug concentration and to reduce the side effects. Additionally, there are two primary routes of clearance of nanoparticles from body. One is the renal filtration with excretion into urine and the other is hepatobiliary (HB) processing with excretion into bile. Clearance of nanoparticles is determined by many factors, including particle size/shape, surface ligand, and surface charge density. Larger particles (>30 nm) are more easily trapped by liver and the RES. Lee et al[40] showed that there was no significant signal change in kidney for SPIONs (>30 nm), indicating that most intravenously injected SPIONs (>30 nm) are captured by liver and spleen, and the elimination of SPION by kidney is limited. Zhang et al[41] also demonstrated that the injected SPIONs with size of 86 nm cannot be metabolized through glomerular filtration. In their studies, the clearance route of 86 nm SPIONs was mainly HB processing with excretion into bile over a period of 14 days. Since SPIO-PEG-D is ~85 nm

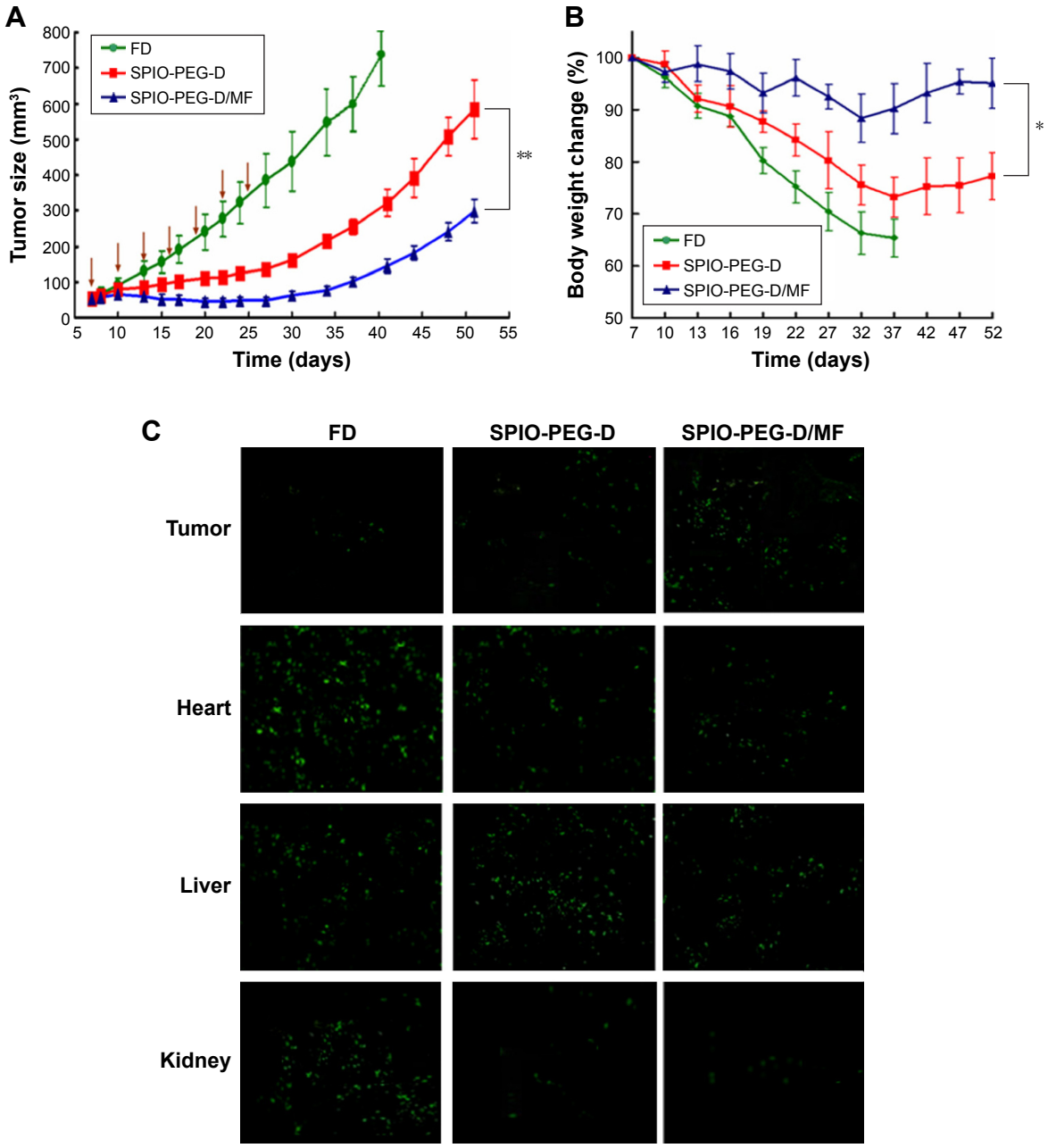

Figure 12 Tumor growth inhibition test of sc HT-29 xenografts in BALB/c nude mice.

Notes: (**A**) Mice were IV injected with SPIO-PEG-D at a dose of 2.5 mg/kg Dox. The administration was carried out seven times with a 3-day interval (arrows: treatment days). (**B**) Body weight changes of the tumor-bearing mice. (**C**) TUNEL analysis of different tissue sections from the tumor-bearing mice treated with different therapeutics at a dose of 2.5 mg/kg Dox on day 40 after HT-29 cell implantation. The administration was carried out seven times with a 3-day interval. Green: apoptotic cells show green fluorescence (mean ± SD [n=4]. *$P<0.05$ and **$P<0.01$).

Abbreviations: sc, subcutaneous; IV, intravenous; SPIO-PEG-D, superparamagnetic iron oxide with polyethylene glycol conjugated with doxorubicin; Dox, doxorubicin; TUNEL, terminal deoxynucleotidyl transferase dUTP nick-end labeling; SD, standard deviation; FD, free doxorubicin; SPIO-PEG-D/MF, SPIO-PEG-D under magnetic field.

in our studies, SPIO-PEG-D is probably eliminated via HB processing with excretion into bile.

Conclusion

In summary, COOH-PEG-triethoxysilane was synthesized, conjugated to the surface of SPIONs to form PEG-bound magnetic nanoparticles (SPIO-PEG), and then Dox was conjugated onto the SPIO-PEG surface to produce SPIO-PEG-D, a multifunctional magnetic nanoparticle. By applying a magnetic field, SPIO-PEG-D could be concentrated in the tumor region to increase the intratumoral concentration of Dox and reduce the drug toxicity for normal organs.

Furthermore, the in vivo MRI study showed that there was a better signal contrast enhancement for SPIO-PEG obtained with applying a magnetic field. This multifunctional magnetic nanoparticle with high loading of drug, superparamagnetic property, and high magnetic relaxivities could become not only an effective delivery system for chemotherapeutic agents but also a great contrast agent for MR imaging. Magnetic enhancement delivery of SPIO-PEG-D was a promising targeting technique that could provide more effective cancer treatment and reduce potential side effects of drug.

Acknowledgments

This work was supported by research grants from the Ministry of Science and Technology of Taiwan (MOST 102-2221-E-002-023-MY3) and the National Health Research Institutes of Taiwan (NHRI BN-104-PP-13).

Disclosure

The authors report no conflicts of interest in this work.

References

1. Xiong D, He Z, An Y, et al. Temperature-responsive multilayered micelles formed from the complexation of PNIPAM-b-P4VP block-copolymer and PS-b-PAA core–shell micelles. *Polymer*. 2008;49:2548–2552.
2. Kim SY, Shin G, Lee YM. Amphiphilic diblock copolymeric nanospheres composed of methoxy poly(ethylene glycol) and glycolide: properties, cytotoxicity and drug release behavior. *Biomaterials*. 1999;20:1033–1042.
3. Li JB, Shi L, An YL, et al. Reverse micelles of star-block copolymer as nanoreactors for preparation of gold nanoparticles. *Polymer*. 2006;47:8480–8487.
4. Kataoka K, Matsumoto T, Yokoyama M, et al. Doxorubicin-loaded poly(ethylene glycol)–poly(β-benzyl-L-aspartate) copolymer micelles: their pharmaceutical characteristics and biological significance. *J Control Release*. 2000;64:143–153.
5. Liu D, Zhong C. Multicompartment micelles formed from star-dendritic triblock copolymers in selective solvents: a dissipative particle dynamics study. *Polymer*. 2008;49:1407–1413.
6. Torchilin VP. Multifunctional nanocarriers. *Adv Drug Deliv Rev*. 2006;58:1532–1555.
7. Kim J, Lee JE, Lee SH, et al. Designed fabrication of a multifunctional polymer nanomedical platform for simultaneous cancer-targeted imaging and magnetically guided drug delivery. *Adv Mater*. 2008;20:478–483.
8. Peer D, Karp JM, Hong S, et al. Nanocarriers as an emerging platform for cancer therapy. *Nat Nanotechnol*. 2007;2:751–760.
9. Nasongkla N, Bey E, Ren J, et al. Multifunctional, polymeric micelles as cancer-targeted, MRI-ultrasensitive drug delivery systems. *Nano Lett*. 2006;6:2427–2430.
10. Yang J, Lee CH, Ko HJ, et al. Multifunctional magneto-polymeric nanohybrids for targeted detection and synergistic therapeutic effects on breast cancer. *Angew Chem Int Ed*. 2007;46:8836–8839.
11. Liong M, Lu J, Kovochich M, et al. Multifunctional inorganic nanoparticles for imaging, targeting, and drug delivery. *ACS Nano*. 2008;2:889–896.
12. Yang X, Grailer JJ, Rowland IJ, et al. Multifunctional SPIO/DOX-loaded wormlike polymer vesicles for cancer therapy and MR imaging. *Biomaterials*. 2010;31:9065–9073.
13. Zhang HZ, Gao FP, Liu LR, et al. Pullulan acetate nanoparticles prepared by solvent diffusion method for epirubicin chemotherapy. *Colloids Surf B Biointerfaces*. 2009;71:19–26.
14. Liu Z, Jiao Y, Wang Y, et al. Polysaccharides-based nanoparticles as drug delivery systems. *Adv Drug Deliv Rev*. 2008;60:1650–1662.
15. Alexiou C, Arnold W, Klein RJ, et al. Locoregional cancer treatment with magnetic drug targeting. *Cancer Res*. 2000;60:6641–6648.
16. Reiss G, Hutten A. Magnetic nanoparticles are useful for a wide range of applications from data storage to medicinal imaging. The large-scale preparation of FeCo nanoparticles boosts this potential. *Nat Mater*. 2005;4:725–726.
17. Qiao R, Jia Q, Hüwel S, et al. Receptor-mediated delivery of magnetic nanoparticles across the blood–brain barrier. *ACS Nano*. 2012;6:3304–3310.
18. Dilnawaz F, Singh A, Mohanty C, et al. Dual drug loaded superparamagnetic iron oxide nanoparticles for targeted cancer therapy. *Biomaterials*. 2010;31:3694–3706.
19. Lubbe AS, Alexiou C, Bergemann C. Clinical applications of magnetic drug targeting. *J Surg Res*. 2001;95:200–206.
20. Häfeli UO. Magnetically modulated therapeutic systems. *Int J Pharm*. 2004;277:19–24.
21. Lübbe AS, Bergemann C, Huhnt W, et al. Preclinical experiences with magnetic drug targeting: tolerance and efficacy. *Cancer Res*. 1996;56:4694–4701.
22. Wang X, Wei F, Liu A, et al. Cancer stem cell labeling using poly(L-lysine)-modified iron oxide nanoparticles. *Biomaterials*. 2012;33(14):3719–3732.
23. Laurent S, Dutz S, Häfeli UO, Mahmoudi M. Magnetic fluid hyperthermia: focus on superparamagnetic iron oxide nanoparticles. *Adv Colloid Interface Sci*. 2011;166(1–2):8–23.
24. Alexiou C, Jurgons R, Schmid RJ, et al. Magnetic drug targeting: biodistribution of the magnetic carrier and the chemotherapeutic agent mitoxantrone after locoregional cancer treatment. *J Drug Target*. 2003;11:139–149.
25. Asmatulu R, Zalich MA, Claus RO, et al. Synthesis, characterization and targeting of biodegradable magnetic nanocomposite particles by external magnetic fields. *J Magn Magn Mater*. 2005;292:108–119.
26. Ma YH, Hsu YW, Chang YJ, et al. Intra-arterial application of magnetic nanoparticles for targeted thrombolytic therapy: a rat embolic model. *J Magn Magn Mater*. 2007;311:34–36.
27. Liu HL, Hua MY, Yang HW, et al. Magnetic resonance monitoring of focused ultrasound/magnetic nanoparticle targeting delivery of therapeutic agents to the brain. *Proc Natl Acad Sci U S A*. 2010;107(34):15205–15210.
28. Lübbe AS, Bergemann C, Riess H, et al. Clinical experiences with magnetic drug targeting: a phase I study with 4′-epidoxorubicin in 14 patients with advanced solid tumors. *Cancer Res*. 1996;56:4686–4693.
29. Owens DE 3rd, Peppas NA. Opsonization, biodistribution, and pharmacokinetics of polymeric nanoparticles. *Int J Pharm*. 2006;307:93–102.
30. Lin JJ, Chen JS, Huang SJ, et al. Folic acid-Pluronic F127 magnetic nanoparticle clusters for combined targeting, diagnosis, and therapy applications. *Biomaterials*. 2009;30:5114–5124.
31. Babic M, Horák D, Jendelová P, et al. Poly(N, N-dimethylacrylamide)-coated maghemite nanoparticles for stem cell labeling. *Bioconjug Chem*. 2009;20:283–294.
32. Chen AL, Ni HC, Wang LF, et al. Biodegradable amphiphilic copolymers based on poly(epsilon-caprolactone)-graft chondroitin sulfate as drug carriers. *Biomacromolecules*. 2008;9:2447–2457.
33. Liu X, Hu Q, Fang Z, et al. Magnetic chitosan nanocomposites: a useful recyclable tool for heavy metal ion removal. *Langmuir*. 2009;25:3–8.
34. Bumb A, Brechbiel M, Chovke PL, et al. Synthesis and characterization of ultra-small superparamagnetic iron oxide nanoparticles thinly coated with silica. *Nanotechnology*. 2008;19:335601.
35. Chertok B, Moffat BA, David AE, et al. Iron oxide nanoparticles as a drug delivery vehicle for MRI monitored magnetic targeting of brain tumors. *Biomaterials*. 2008;29:487–496.

36. Liu CG, Desai KG, Chen XG, et al. Linolenic acid-modified chitosan for formation of self-assembled nanoparticles. *J Agric Food Chem*. 2005; 53:437–441.
37. Imai Y, Murakami T, Yoshida S, et al. Superparamagnetic iron oxide-enhanced magnetic resonance images of hepatocellular carcinoma: correlation with histological grading. *Hepatology*. 2000;32:205–212.
38. Ward J, Guthrie JA, Scott DJ, et al. Hepatocellular carcinoma in the cirrhotic liver: double-contrast MR imaging for diagnosis. *Radiology*. 2000; 216:154–162.
39. Hori M, Murakami T, Kim T, et al. Detection of hypervascular hepatocellular carcinoma: comparison of SPIO-enhanced MRI with dynamic helical CT. *J Comput Assist Tomogr*. 2002;26:701–710.
40. Lee PW, Hsu SH, Wang JJ, et al. The characteristics, biodistribution, magnetic resonance imaging and biodegradability of superparamagnetic core–shell nanoparticles. *Biomaterials*. 2010;31:1316–1324.
41. Zhang B, Li Q, Yin P, et al. Ultrasound-triggered BSA/SPION hybrid nanoclusters for liver-specific magnetic resonance imaging. *ACS Appl Mater Interfaces*. 2012;4:6479–6486.